

PAPER

Underwater anechoic layer with parallel metallic plate insertions: theoretical modelling

To cite this article: Chenlei Yu *et al* 2021 *J. Micromech. Microeng.* **31** 074002

View the [article online](#) for updates and enhancements.

You may also like

- [Metallic spherical anechoic chamber for antenna pattern measurement](#)
Ali Farahbakhsh and Mohammad Khalaj-Amirhosseini
- [Observation of semi anechoic room influence on high frequency antenna measurements](#)
M Pospisilik, M Adamek, P Neumann *et al.*
- [The correlation of EDT and T30 result of YMEC measurement compared with RT Sabine theory and Eyring in semi-anechoic room in physics department Institut Teknologi Sepuluh Nopember](#)
Susilo Indrawati, Melania Suweni Muntini, Iim Fatimah *et al.*



IOP | ebooks™

Bringing together innovative digital publishing with leading authors from the global scientific community.

Start exploring the collection—download the first chapter of every title for free.

Underwater anechoic layer with parallel metallic plate insertions: theoretical modelling

Chenlei Yu^{1,2,3}, Mingyu Duan^{1,2} , Wei He^{1,2}, Fengxian Xin^{1,2,*}  and Tian Jian Lu^{3,4,*}

¹ State Key Laboratory for Strength and Vibration of Mechanical Structures, Xi'an Jiaotong University, Xi'an 710049, People's Republic of China

² MOE Key Laboratory for Multifunctional Materials and Structures, Xi'an Jiaotong University, Xi'an 710049, People's Republic of China

³ State Key Laboratory for Mechanics and Control of Mechanical Structures, Nanjing University of Aeronautics and Astronautics, Nanjing 210016, People's Republic of China

⁴ MIIT Key Laboratory of Multi-functional Lightweight Materials and Structures, Nanjing University of Aeronautics and Astronautics, Nanjing 210016, People's Republic of China

E-mail: fengxian.xin@gmail.com and tjlu@nuaa.edu.cn

Received 24 February 2021, revised 5 May 2021

Accepted for publication 25 May 2021

Published 9 June 2021



Abstract

A novel underwater composite anechoic layer is proposed by inserting periodically placed longitudinal parallel steel plates into a viscoelastic rubber matrix. Built upon the complex viscosity model of viscoelastic materials, a theoretical model is established to evaluate the sound absorption performance of the proposed anechoic layer. For validation, finite element simulations are carried out, and good agreements are achieved between theory and simulation. Compared with the reference structure purely made of rubber, the new anechoic layer exhibits greatly improved sound absorption performance. It is demonstrated that the steel plate insertions significantly enlarge the shear deformation of rubber at plate–rubber interfaces, causing greatly improved viscous dissipation of acoustic energy. Systematic variations of material properties and geometrical parameters reveal the dominant roles of rubber viscosity and plate spacing. Further, a theoretical model is developed to study the effect of non-tight connection at rubber–plate interfaces. This study broadens the application scope of the complex viscosity model and provides useful guidance for designing novel anechoic layers with tailored underwater acoustic performances.

Keywords: underwater sound absorption, complex viscosity model, rubber, parallel plates

(Some figures may appear in colour only in the online journal)

1. Introduction

Underwater acoustic stealth technology is an important means for underwater vehicles to avoid sonar detection. At present, the most effective method is to cover an anechoic layer on a target object to absorb incident sound waves [1–3]. To achieve good stealth performance, the characteristic impedance of the anechoic layer should be close to that of water for

reduced reflection. Viscoelastic materials such as rubber and polyurethane have acoustic impedance similar to water and hence are often used to construct underwater sound absorbers. When a sound wave is incident, the friction between molecules of the viscoelastic material consumes part of the acoustic energy, and the intensity of the sound wave decreases with increasing propagation distance [4]. Experiments show that, for viscoelastic materials, the energy dissipated via shear deformation is much larger than that dissipated via compressive deformation [4–9]. In particular, when the Poisson ratio of the viscoelastic material is close to 0.5, it is almost

* Authors to whom any correspondence should be addressed.

incompressible, so energy dissipation caused by compressive deformation is negligible [5].

Existing researches of anechoic layers have mainly focused on composite structures with air cavities [1, 5, 10–14] or local resonators [2, 15–21]. For the former, cavity resonance enhances vibration of the viscoelastic material, with more acoustic energy converted into useless heat [1]. However, due to the deformation of the anechoic layer with cavities under the action of hydraulic pressure, the sound-absorption performance deteriorates with the increase of service depth [22]. In contrast, a local resonant cavity is composed of a heavy core and a soft viscoelastic material. Near the resonance frequency, vibration of the nucleus enhances friction between molecules, thereby increasing acoustic energy dissipation [15]. However, at present, the sound absorption bandwidth of a typical local resonance anechoic layer remains relatively narrow, thereby requiring further broadband design for practical applications.

This paper proposes a new type of underwater anechoic layer, which is constructed by inserting periodically placed longitudinal parallel steel plates into a rubber matrix. In the process of sound wave propagation, molecular friction inside the viscoelastic rubber is enhanced by steel plate insertions that are well bonded to the rubber, thus enabling more acoustic energy to be dissipated. Typically, the properties of a viscoelastic material lie between elastic solid and viscous fluid. Solid viscoelastic materials, such as rubber and polyurethane, are usually characterized by the complex modulus model [6, 17], while liquid viscoelastic materials, such as blood and petroleum, are commonly characterized by the complex viscosity model [23]. Under the condition of equal dissipated energy, the complex modulus model and the complex viscosity model for viscoelastic materials can be converted to each other [24]. Due to the presence of shear waves in a viscoelastic material, it is difficult to describe the propagation of sound waves using the complex modulus model. To address this issue, in the present study, the complex viscosity model is employed for the first time to predict the sound absorption performance of the proposed composite anechoic layer. For validation, a finite element (FE) numerical model is established. The FE simulation results are compared with the theoretical predictions, with good agreements achieved. The validated theoretical model is subsequently used to explore energy dissipation of the viscoelastic material (rubber) as well as sound absorption mechanisms of the proposed anechoic layer, and quantify the influence of key material properties and geometric parameters on sound absorption. Finally, to understand how imperfect connections between rubber matrix and plate insertions may affect the acoustic performance of the composite structure, a simplified model is established, with its predictions also validated against FE simulation results.

2. Theory

2.1. Anechoic layer with inserted parallel plates

Figure 1(a) presents schematically an infinite anechoic layer constructed by inserting parallel steel plates into a viscoelastic rubber matrix, periodic in the x -direction and infinitely long

in the y -direction. One side of the anechoic layer is water, the other side is fixed on a rigid wall, and a plane sound wave traveling in the water is vertically incident onto the surface of the proposed composite structure. A two-dimensional (2D) view of its periodic cell is displayed in figure 1(b). Let h denote the thickness of the composite anechoic layer, a denote the plate spacing, and t represent the plate thickness. The volume proportion of rubber in the anechoic layer is $\phi = 1 - t/(t + a)$. Unless otherwise stated, it is assumed that the steel plates are tightly bound to the rubber and no slip occurs at steel-rubber interfaces. Since the stiffness of steel is hundreds of times greater than that of rubber, the plates are assumed to be rigid in subsequent theoretical modeling.

2.2. Complex viscosity model of viscoelastic material

To establish a complex viscosity model for a viscoelastic material (e.g. rubber), consider first a 2D case, as shown figure 2. A particle in the viscoelastic material moves a distance ξ along the z -axis, governed by [25]:

$$\rho \frac{\partial^2 \xi}{\partial t^2} = (\lambda + 2G) \frac{\partial^2 \xi}{\partial z^2} + G \frac{\partial^2 \xi}{\partial x^2} + \mu_1 \frac{\partial^3 \xi}{\partial z^2 \partial t} + \mu_s \frac{\partial^3 \xi}{\partial x^2 \partial t} \quad (1)$$

where ρ is the density, t is time, λ and G represent two Lamé constants, and μ_1 and μ_s are the volume and shear viscosity, respectively. On the right-hand side, the first and second terms represent elastic forces, while the third and fourth terms represent viscous forces. When the effect of viscosity is negligible, equation (1) degenerates into the traditional elasticity form.

Under the excitation of a harmonic sound wave, the displacement ξ can be expressed as:

$$\xi = \xi(x, z) \cdot e^{j\omega t} \quad (2)$$

where $j = \sqrt{-1}$ is the imaginary unit and ω is the angular frequency. Substituting (2) into (1) leads to:

$$-\rho\omega^2 \xi(x, z) = [(\lambda + 2G) + j\omega\mu_1] \frac{\partial^2 \xi(x, z)}{\partial z^2} + (G + j\omega\mu_s) \frac{\partial^2 \xi(x, z)}{\partial x^2} \quad (3)$$

where $K_c = (\lambda + 2G) + j\omega\mu_1$ and $G_c = G + j\omega\mu_s$ are the complex bulk and shear moduli. In practical applications, the material parameters of a typical viscoelastic material such as rubber are often given by wave speeds, so that:

$$\begin{aligned} K_c &= c_1^2(1 + j\eta_1)\rho \\ G_c &= c_s^2(1 + j\eta_s)\rho \end{aligned} \quad (4)$$

where c_1 and c_s are the compressional and shear wave speeds, and η_1 and η_s are referred to as the loss factors of the bulk and shear moduli.

Upon expressing the last term of (3) in terms of viscosity as $j\omega \left(\mu_s - \frac{jG}{\omega} \right) \frac{\partial^2 \xi(x, z)}{\partial x^2}$, equation (3) exhibits the same form as the governing equation of fluids, thus implying that the

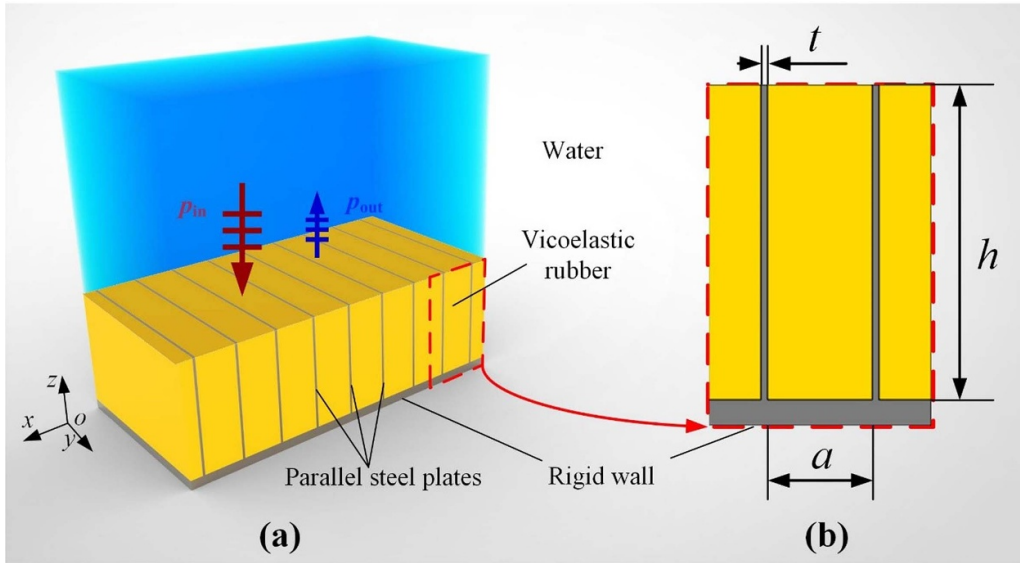


Figure 1. (a) Schematic of proposed composite anechoic layer with longitudinal parallel plate insertions, and (b) 2D view of its periodic cell (unit cell).

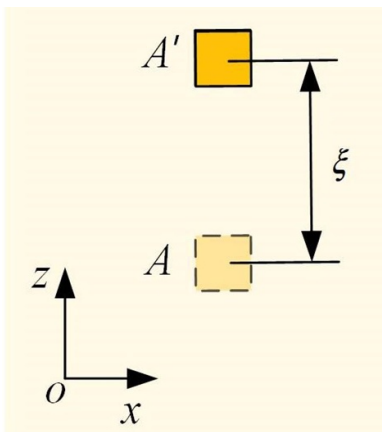


Figure 2. A particle moves along the z -axis in a viscoelastic material (e.g. rubber).

viscoelastic material may be treated as a fluid. Its complex viscosity μ_c is thence related to its complex shear modulus G_c , as [24]:

$$\mu_c = -j \cdot \frac{G_c}{\omega}. \quad (5)$$

2.3. Characteristics of acoustic propagation in parallel slits

Upon using the complex viscosity model (as described in the previous section) to describe the vibration of rubber under acoustic excitation, propagation of the sound wave in the proposed anechoic layer of figure 1 can be regarded as wave propagation in parallel slits. Figure 3 displays a single slit of spacing a , wherein the sound wave travels along the z -direction in the equivalent fluid (i.e. rubber). In this case, the governing equation can be expressed as [26]:

$$j\omega\rho u = -\frac{\partial p}{\partial z} + \mu_c \frac{\partial^2 u}{\partial x^2} \quad (6)$$

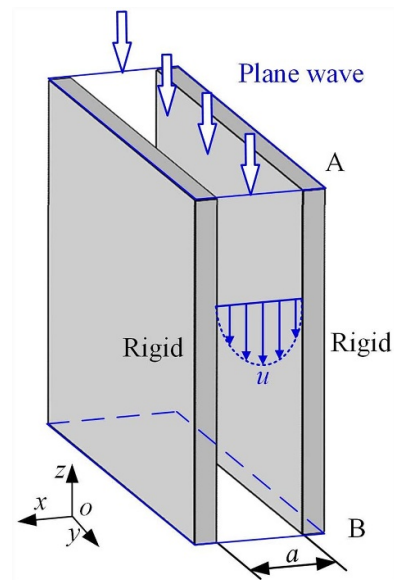


Figure 3. Plane-wave transmitted in parallel rigid plates.

where u is the velocity and p is the sound pressure.

With no-slip condition $u = 0$ when $y = 0$ and $y = a$, equation (6) can be solved as:

$$u = -\frac{1}{j\omega\rho} \frac{\partial p}{\partial z} \left[1 - \frac{\cosh(x\sqrt{j\omega\rho/\mu_c})}{\cosh(a\sqrt{j\omega\rho/\mu_c}/2)} \right]. \quad (7)$$

By averaging the above formula in the x -direction, the average velocity of the medium between the two parallel rigid plates can be obtained [26], as:

$$\bar{u} = -\frac{1}{j\omega\rho} \frac{\partial p}{\partial z} \left[1 - \frac{1}{Q\sqrt{j}} \tanh(Q\sqrt{j}) \right] \quad (8)$$

where $Q = \frac{a}{2} \sqrt{\omega \rho / \mu_c}$ reflects the ratio of plate spacing to viscous boundary layer thickness $\delta = \sqrt{2\mu_c / (\omega \cdot \rho)}$.

With the effective density ρ_{eq} expressed as:

$$\rho_{eq} = \rho \left[1 - \frac{1}{Q\sqrt{j}} \tanh(Q\sqrt{j}) \right]^{-1}. \quad (9)$$

Equation (8) can be transformed into $j\omega\rho_{eq}\bar{u} = -\partial p / \partial z$.

Concerning the entrance surface A and the exit surface B of the anechoic layer, the relationship between the sound pressure and the velocity can be obtained as:

$$\begin{bmatrix} p(A) \\ \bar{u}(A) \end{bmatrix} = \begin{bmatrix} 1 & 0 \\ 0 & \phi \end{bmatrix} [T] \begin{bmatrix} p(B) \\ \bar{u}(B) \end{bmatrix} \quad (10)$$

where $T = \begin{bmatrix} \cosh kh & jZ_c \sinh kh \\ j \sinh kh / Z_c & \cosh kh \end{bmatrix}$ is the transfer matrix of the anechoic layer, in which $Z_c = \sqrt{K_c \rho_{eq}}$ is the characteristic impedance and $k = \omega \sqrt{\rho_{eq} / K_c}$ represents the wavenumber of the anechoic layer.

The anechoic layer is backed by a rigid wall, thus $\bar{u}(B) = 0$. Its surface acoustic impedance can be obtained by:

$$Z_s = \frac{p(A)}{\bar{u}(A)} = \frac{Z_c \cosh kh}{\phi j \sinh kh}. \quad (11)$$

Finally, the sound absorption coefficient of the proposed composite anechoic layer is calculated as:

$$\alpha = 1 - \left| \frac{Z_s - Z_0}{Z_s + Z_0} \right|^2 \quad (12)$$

where $Z_0 = \rho_0 c_0$ is the characteristic impedance of water, ρ_0 is the density of water, and c_0 is the sound speed in the water.

3. Numerical model

To validate the present analytical model, a 2D numerical model, as shown in figure 4, is established using the commercial FE code COMSOL [27]. From top to down are the perfectly matched layer (PML), the water, and the anechoic layer, respectively. The PML is a domain that can absorb all the waves entering into it, thus is added to the end of the water to simulate the infinite acoustic domain. The water is considered as a compressible but lossless fluid with no thermal conductivity and viscosity, which is governed by the Helmholtz equation:

$$\nabla^2 p = \frac{1}{c_0^2} \frac{\partial^2 p}{\partial t^2}. \quad (13)$$

The anechoic layer is simulated using the solid mechanics modulus of COMSOL, with the following control equation:

$$-\rho\omega^2 \mathbf{s} - \frac{1}{2} \nabla \cdot \mathbf{C} : ((\nabla \mathbf{s})^T + \nabla \mathbf{s}) = 0 \quad (14)$$

where ρ and \mathbf{s} represent the density and displacement of the solid, respectively, and \mathbf{C} is the viscoelastic tensor.

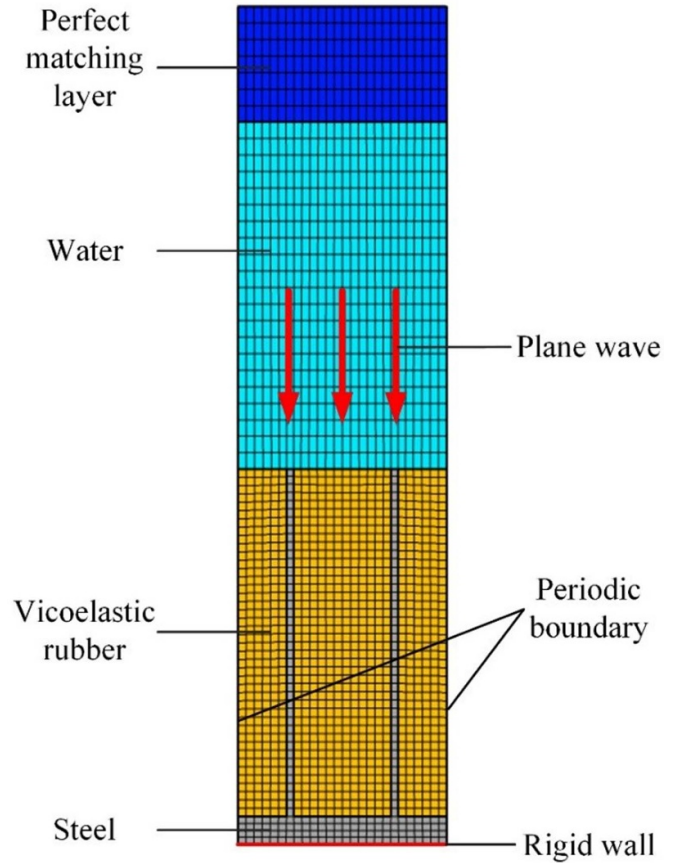


Figure 4. FE model of the proposed composite anechoic layer for underwater sound absorption.

At solid–fluid interfaces, the normal accelerations of the water and the anechoic layer are continuous, requiring:

$$-\mathbf{n} \cdot \left(-\frac{1}{\rho_0} \nabla p \right) = -\mathbf{n} \cdot \mathbf{s}_{tt} \quad (15)$$

where \mathbf{n} is the surface normal and \mathbf{s}_{tt} is the acceleration of solid. The load experienced by the solid is:

$$\mathbf{F}_A = p_t \mathbf{n} \quad (16)$$

where p_t is the total acoustic pressure.

Finally, the sound absorption coefficient of the anechoic layer is calculated by:

$$\alpha = 1 - R^2 \quad (17)$$

where $R = \langle p_s \rangle / \langle p_b \rangle$ is the sound pressure reflection coefficient, p_b and p_s are the background sound pressure and scattered sound pressure of the incident surface, respectively, and $\langle \cdot \rangle$ represents the average over the incident surface.

Table 1. Physical parameters of rubber [6].

Material parameter	ρ	c_1	η	c_s	η_s
Value	1000 kg m^{-3}	1000 m s^{-1}	0.09	100 m s^{-1}	0.9

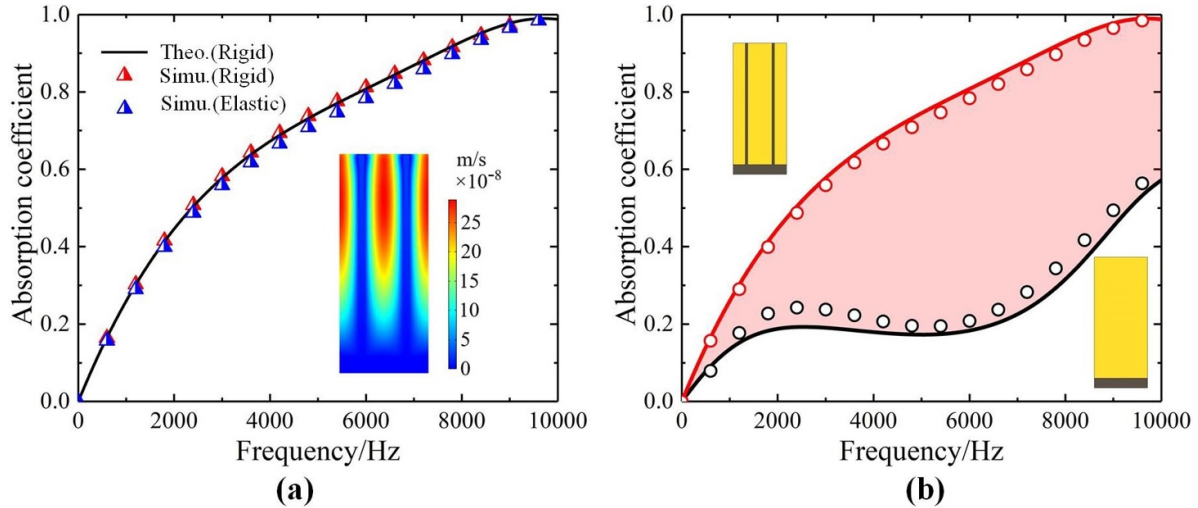


Figure 5. (a) Sound absorption coefficients predicted by theoretical model (black curve), FE model with rigid plates (red triangles) and FE model with elastic steel plates (blue triangles). The inlet shows the vibration velocity distribution in solid domains (steel and rubber) at 4000 Hz. (b) theoretical predicted and numerically calculated sound absorption coefficients plotted as functions of frequency for anechoic layer with/without inserted steel plates. Solid lines represent theoretical predictions while circles represent simulation results.

4. Results and discussion

4.1. Sound absorption performance of the proposed composite anechoic layer

Underwater sound absorption performance of the proposed anechoic layer is compared with that without inserted longitudinal parallel plates, i.e. a pure rubber layer for reference. Relevant physical parameters of the rubber considered are listed in table 1 which, for simplicity, are assumed to be constant over the whole frequency range [6, 7, 12, 18]. The density and sound speed of the water are 1000 kg m^{-3} and 1500 m s^{-1} . The steel selected has density 7850 kg m^{-3} , Young’s modulus 209 GPa, and Poisson ratio 0.3. Concerning representative underwater applications, the thickness of the proposed anechoic layer is taken as $h = 50 \text{ mm}$, while plate spacing a is set to 10 mm and plate thickness t is chosen as 1 mm. Under such conditions, the volume proportion of rubber is $\phi = 0.91$ in the anechoic layer.

To verify the assumption of rigid plate insertions and the theoretical prediction of the complex viscosity model, we compared the sound absorption coefficients predicted by theoretical model, FE model with rigid plates, and FE model with elastic steel plates in figure 5(a). It can be seen that the simulated sound absorption coefficients are in good agreements with the theoretical prediction in the studied frequency range, demonstrating that the complex viscosity model can accurately describe the underwater sound absorption performance of viscoelastic materials. In addition, compared with the FE model based on the rigid plates, the sound absorption

coefficient of the complete FE model considering the elastic plate is also basically consistent with the theoretical prediction. The difference is that the absorption coefficient of the FE model considering elastic plates is slightly lower, but the error is less than 10%. This can be explained by the coupling vibration of the steel plates and rubber. However, the stiffness of the steel plates in the direction of sound propagation is much greater than that of rubber, and the particle vibration velocity in steel plates is almost 0 compared with rubber, as shown in the inlet. That is, the assumption of rigid plate insertions in the theoretical model is valid here.

Figure 5(b) compares the theoretically predicted and numerically simulated sound absorption coefficients of the anechoic layer, with and without longitudinal parallel steel plate insertions. The results demonstrate that the anechoic layer with inserted parallel plates exhibits much superior acoustic performance relative to a pure rubber layer. For the case considered, the maximum improvement of sound absorption coefficient is 0.62 at 7043 Hz while the average sound absorption coefficient over the whole frequency range considered (i.e. from 0 to 10000 Hz) is increased from 0.25 to 0.68.

To understand why inserting parallel steel plates into a rubber matrix leads to enhanced sound absorption, figures 6(a) and (b) compare energy dissipated by the proposed anechoic layer with inserted plates with that without such insertions at 4000 Hz; at other frequencies the trend is similar, thus not shown here for brevity. For the latter (i.e. a pure rubber layer without insertions), the energy dissipation varies slightly from top to down. In sharp contrast, on both sides of a plate

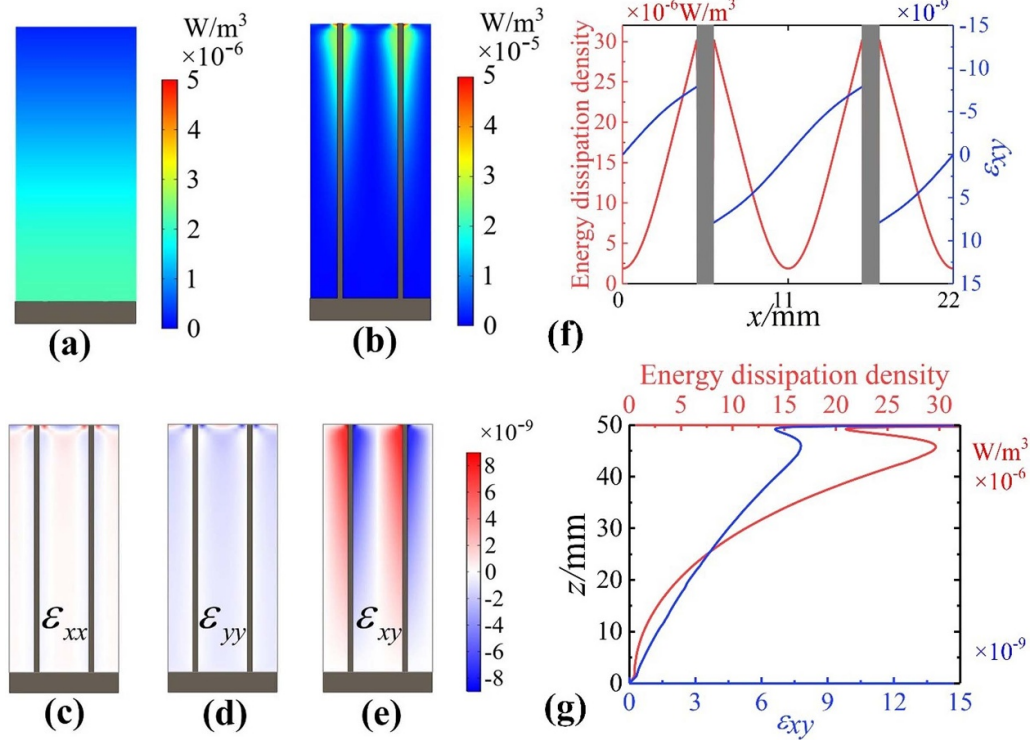


Figure 6. Numerically simulated results for energy dissipation of anechoic layer at 4000 Hz: (a) without inserted plates and (b) with inserted plates. Distribution of strain in viscoelastic rubber at 4000 Hz: (c) ϵ_{xx} , (d) ϵ_{yy} and (e) ϵ_{xy} . Distribution of energy dissipation density and shear strain on (f) a selected cross-section 5 mm (i.e. $z = 45$ mm) away from entrance and (g) rubber–plate interface.

insertion, the energy dissipated by rubber increases by more than ten times, especially near the top where the sound wave is incident. This is mainly attributed to intense shear deformation occurring at the rubber–plate interfaces, as elucidated below. For a composite anechoic layer with inserted plates, figures 6(c)–(e) display strain fields in the rubber matrix at 4000 Hz, with ϵ_{xx} and ϵ_{yy} representing the normal strains and ϵ_{xy} the shear strain. Near the rubber–plate interfaces, it is seen that the shear strain is much greater than the normal ones, especially towards the top of the anechoic layer. In other words, inserting steel plates into the rubber enhances its shear deformation near the interfaces, thus dissipating more acoustic energy. For more quantitative evaluation, figure 6(f) presents the section having the highest energy dissipation density and shear strain, which is 5 mm (i.e. $z = 45$ mm) away from the surface of the anechoic layer, while figure 6(g) presents the distribution of energy dissipation density and shear strain on the rubber–plate interface. Along the x -direction, as shown in figure 6(g), the energy dissipation density at the midmost position between the two plates is the smallest, where the shear strain is zero due to symmetry. The closer to an inserted plate, the stronger the shear strain and the greater the energy loss density. Given that rubber vibration near the bottom is constrained by the fixed backplate, shear deformation (and hence energy dissipation) gradually decreases from top to bottom, as illustrated in figure 6(g). Note that shear strain at the entrance (i.e. $z = 50$ mm) is also small, for no shear force is present on the top surface of the anechoic layer.

4.2. Influence of material parameters on the absorption coefficient

The physical properties of rubber can be tailored by changing the composition of molecular chains or adding organic/inorganic particles. For instance, the compression wave speed in silicone rubber is less than 100 m s^{-1} but exceeds 1000 m s^{-1} in butyl rubber. To provide guidance for material selection, the proposed theoretical model is utilized to evaluate how rubber material parameters affect the acoustic performance of the proposed anechoic layer. Unless otherwise indicated, the remaining parameters of the model are fixed as those presented in the previous section.

The acoustic impedance of an anechoic layer dictates the ability of a sound wave to enter it from water, which is proportional to its density and compressive wave speed. As decreasing the acoustic impedance makes it easier for the sound to enter the anechoic layer at relatively low frequencies, the density and compressive wave speed of rubber have similar effects on the absorption performance of the structure. When the rubber density or compressive wave speed is reduced, the sound absorption coefficient is increased at lower frequencies, as illustrated by the results shown in figures 7(a) and (b). It is seen that, because energy dissipation is mainly caused by shear deformation, the influence of compressive wave speed is relatively small compared with that of shear wave. Further, as shown in equation (5), the viscosity coefficient of rubber is proportional to its shear modulus. Therefore, rubber viscosity increases with shear wave speed, enabling the sound

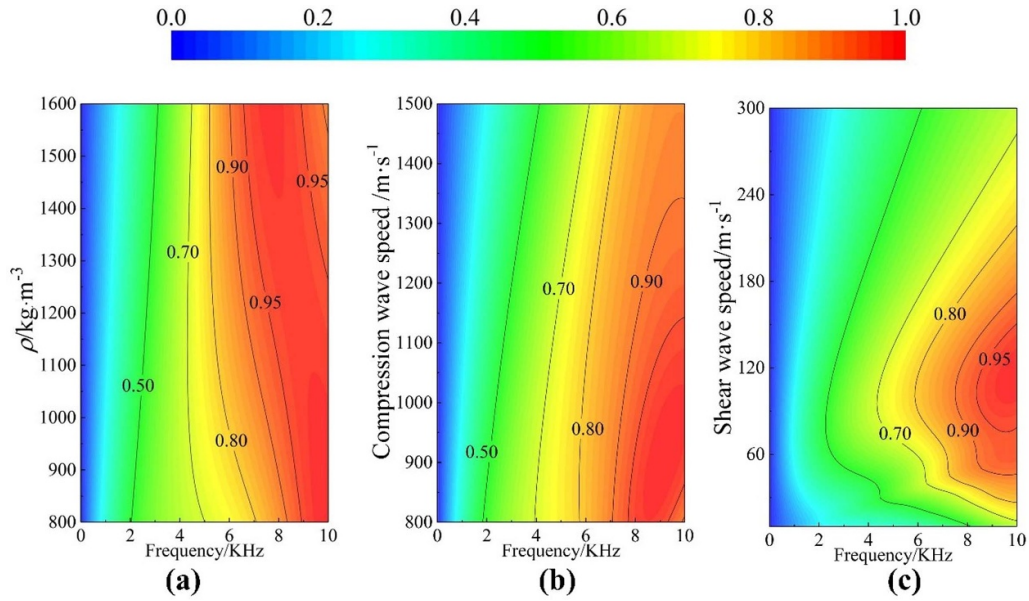


Figure 7. Influence of rubber properties on the absorption coefficient of composite anechoic layer with inserted plates: (a) density, (b) compression wave speed, and (c) shear wave speed.

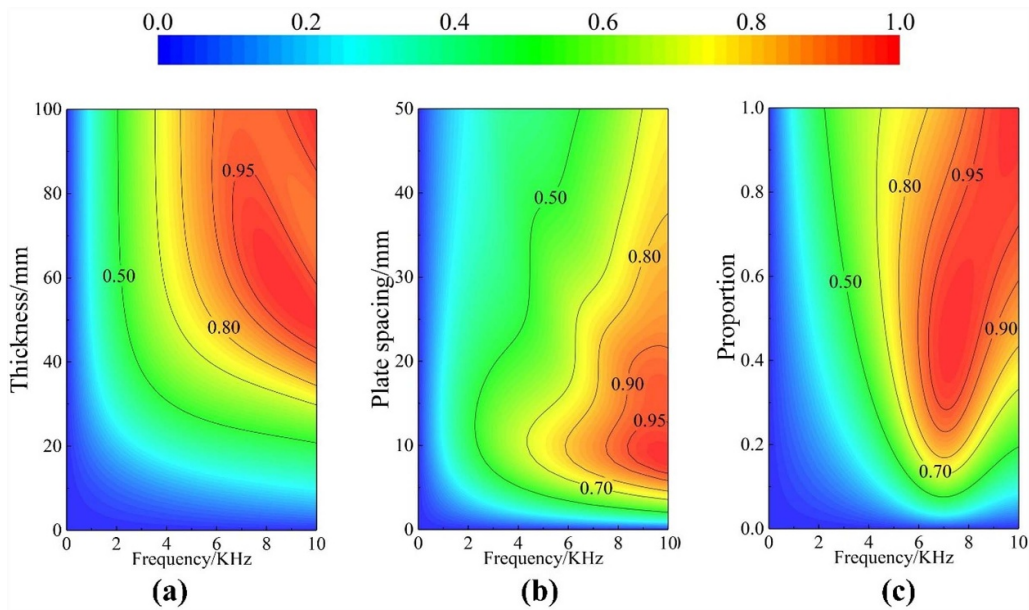


Figure 8. Influence of geometrical parameters on the absorption coefficient of composite anechoic layer with inserted plates: (a) thickness of the anechoic layer, (b) plate spacing, and (c) proportion of rubber.

absorption coefficient to increase accordingly. Nonetheless, as excessive viscosity would also hinder rubber vibration, the absorption coefficient increases first and then decreases with increasing shear wave speed, irrespective of the frequency considered, as shown in figure 7(c).

4.3. Influence of geometrical parameters on the absorption coefficient

In addition to rubber properties, the influence of geometrical parameters is also quantified using the proposed theoretical model, as shown in figure 8. Figure 8(a) illustrates the variation

of sound absorption spectrum with anechoic layer thickness. Similar to the case of a homogeneous rubber layer without plate insertions, increasing the thickness elevates the absorption coefficient of the proposed anechoic layer over the entire frequency range. However, for the parameters considered herein, when the thickness is increased beyond 60 mm, the absorption coefficient hardly changes, suggesting that there exists a propagation limit of sound in the anechoic layer. The effect of plate spacing on sound absorption is exactly opposite to that of shear wave speed, as demonstrated in figure 8(b). Intuitively, the smaller the plate spacing, the more difficult the sound wave propagation. In the extreme case when the plate

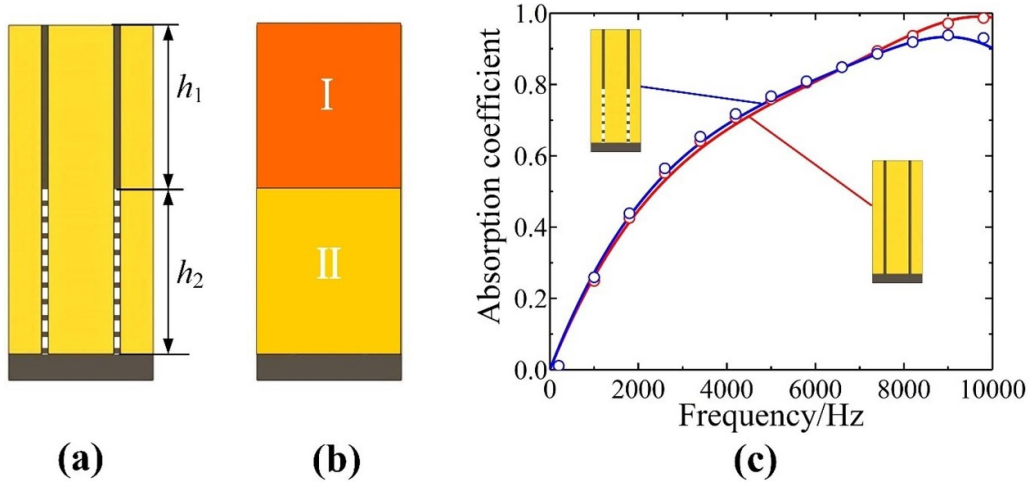


Figure 9. (a) 2D view of composite anechoic layer with a defective segment and (b) the equivalent model. (c) Theoretical and numerical results for sound absorption coefficient of anechoic layer with/without defective segment. Solid line represents theoretical predictions, while circles represent FE simulation results.

spacing approaches 0, the anechoic layer can no longer absorb sound, as can be seen from figure 8(b). Figure 8(c) reveals the relationship between the sound absorption and the proportion of rubber. With other conditions unchanged, the sound absorption performance of the anechoic layer increases with increasing rubber proportion, especially at relatively low frequencies.

4.4. Influence of non-tight connection between rubber and plate insertions

The previous analyses are based on the assumption that the rubber matrix is perfectly bonded to the plate insertions. In practice, however, imperfect bonding between the two during preparation. To understand how such interfacial defect may affect the acoustic performance of the anechoic layer, a simplified model is developed as shown in figure 9(a) where the plate insertions are not bonded to the rubber along a segment of length h_2 at the bottom of the structure. Built upon the analyses of section 2.3, the model of figure 9(a) may be approximated as equivalent to a two-layer homogenized model shown in figure 9(b). With no shear force at the non-tightly connected interface assumed, the density of region II is the density of rubber, while the density of region I is calculated by equation (9). In such case, the transfer matrix of the anechoic layer in equation (10) is replaced by:

$$[T] = [T_I][T_{II}] \tag{18}$$

where $[T_I]$ and $[T_{II}]$ are the transfer matrices of the two homogeneous media, respectively. The sound absorption coefficient of the anechoic layer having interfacial defect can thence be obtained from equation (12). The simulation is consistent with the previous case (no presence of defect), except that the interface condition at the non-tightly connected interface in region II is changed to $\mathbf{s} \cdot \mathbf{n} = 0$, that is, no z -direction constraints. In addition to carrying out the theoretical analysis, FE simulation is also performed to validate such analysis.

The material and geometrical parameters of the model are the same as those presented in section 4.1. For simplicity, the

two segments are assumed to have identical thickness, with $h_1 = h_2 = h/2$. As shown in figure 9(c), the sound absorption coefficient of the anechoic layer with a defective segment (blue curve) is compared with that of the complete section (red curve). It is seen that the theoretical prediction (solid line) agrees well with the FE simulation result (circle). The results show further that the existence of defective segment has non-negligible effect on sound absorption. Sound absorption performance in the low-frequency range is slightly improved, while that in the high-frequency range is significantly reduced.

To gain a fundamental understanding for the influence of non-tight connection, figures 10(a) and (b) present FE simulation results for shear strain and energy dissipation of the anechoic layer with a defective segment, at 4000 Hz. It can be seen that there is no shear strain in the defect section, so there is almost no energy dissipation. Since the rubber at the non-tightly connected interface is not restricted by the z -direction of the wall, its deformation increases under the action of sound waves, resulting in increased shear strain and energy dissipation of the defect-free rubber. Moreover, there is a strong stress concentration at the junction of different segments, as shown in figure 10(c). Compared with the anechoic layer in the defect-free section in figure 6(g), the shear strain and energy dissipation of the anechoic layer in the defect section of the rubber-plate interface appear two characteristics: the defect-free section is enhanced, and the defective section is almost zero. These two differences determine the effect of defects on sound absorption performance. In figures 10(d) and (e), the energy dissipation between the anechoic layer with/without the defective segment at 2000 and 8000 Hz are compared. In the low-frequency range, the energy dissipation enhancement of the defect-free section dominates, thereby improving the sound absorption performance. In the high-frequency range, the energy dissipation of the defective section generally decreases, and the sound absorption performance decreases.

Consider next the influence of the location and length of the defective segment on sound absorption. To this end, based

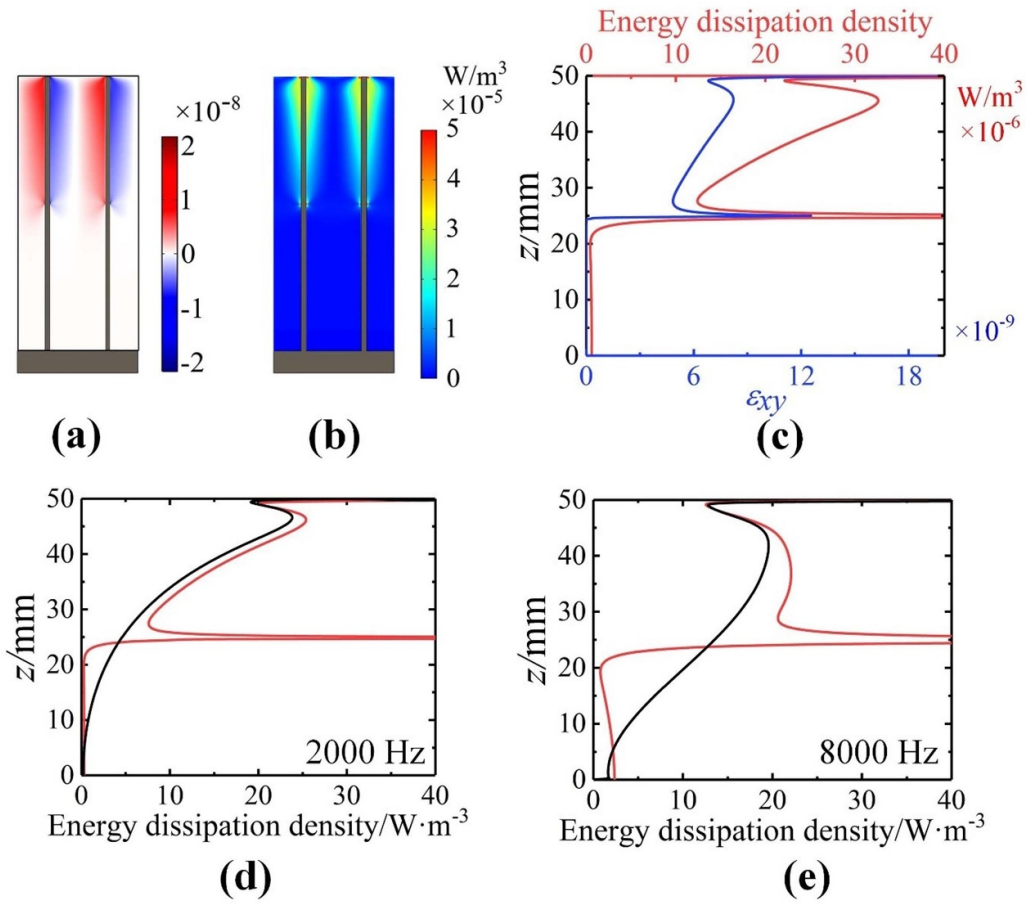


Figure 10. Numerical simulation results of (a) shear strain and (b) energy dissipation at 4000 Hz in composite anechoic layer with interfacial defect. (c) Energy dissipation density and shear strain distribution at 4000 Hz on rubber–plate interface of anechoic layer with interfacial defect. Comparison of energy dissipation of anechoic layer with/without defects at (d) 2000 Hz and (e) 8000 Hz.

on the two-layer model, a three-layer model is established wherein the defective segment is the middle layer, as shown in the inlet of figure 11. Let h_2 denote the length of the defective segment and let h_3 denote the distance of the defective segment to the bottom of the anechoic layer. Similar to the two-layer model, the transfer matrix is obtained by multiplying the transfer matrix of the three equivalent layers.

By fixing the length of the defective segment to $h_2 = 25$ mm but changing h_3 , the predicted sound absorption curves using the three-layer model are plotted in figure 11(a). It is seen that, as h_3 is increased, the sound absorption curve hardly changes below 2000 Hz, but moves downward above 2000 Hz. This occurs because the most serious influence of interfacial defects on the present anechoic layer is that the energy dissipation density of the defective segment is reduced to 0, while the energy dissipation density of the upper part of the anechoic layer is enlarged. Therefore, the closer the defective segment to the top, the worse the sound absorption coefficient. That is, the upper part of the anechoic layer is more sensitive to interfacial defects.

With the defect center fixed at the midpoint of the anechoic layer, the influence of defect length h_2 on sound absorption is presented in figure 11(b). Comparing the

three curves reveals that, as the length of defective segment is increased, sound absorption performance gradually deteriorates, especially at high frequencies. The reason is similar to that discussed above for figure 11(a), i.e. the sound absorbing capability of the anechoic layer is weakened as the invalid area caused by defective segment is enlarged.

The previous discussion focused on the internal situation of the defective segment, but when the defective segment is located at the top, the influence on the sound absorption performance is different. By changing the defect length h_2 of the top defective segment, the predicted sound absorption curves are plotted in figure 12. It can be seen that as the defect length h_2 increases, the sound absorption coefficients decrease globally in the studied frequency range. Because the top layer is not constrained by the steel plate, its acoustic performance is consistent with that of uniform rubber, that is, the anechoic layer with top defective segment can be regarded as a connection of uniform rubber layer and an anechoic layer with steel plate insertions. The acoustic energy is mainly dissipated by the lower anechoic layer with steel plate insertions, and its thickness is decreased by the top defect. Therefore, the influence of the top defective segment on the sound absorption

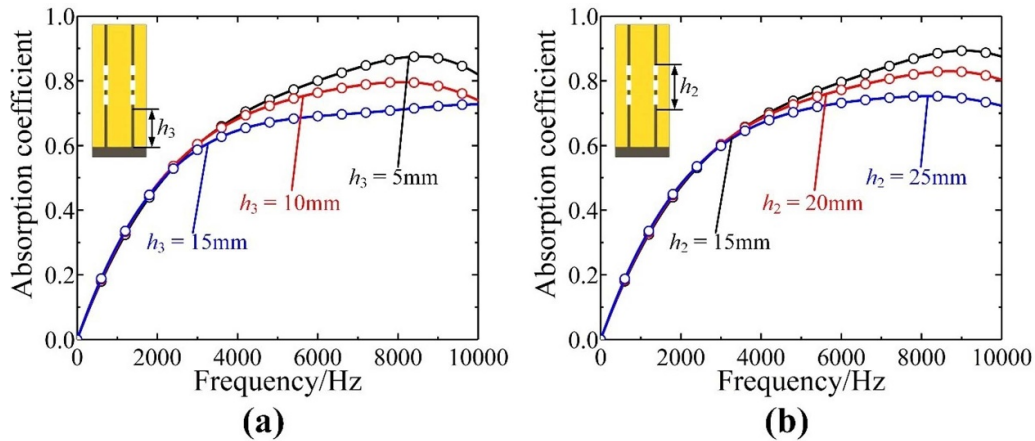


Figure 11. (a) Influence of (a) location of defective segment (length of defect fixed at 25 mm) and (b) length of defective segment (center of defective segment fixed at midmost position of anechoic layer) on sound absorption coefficient.

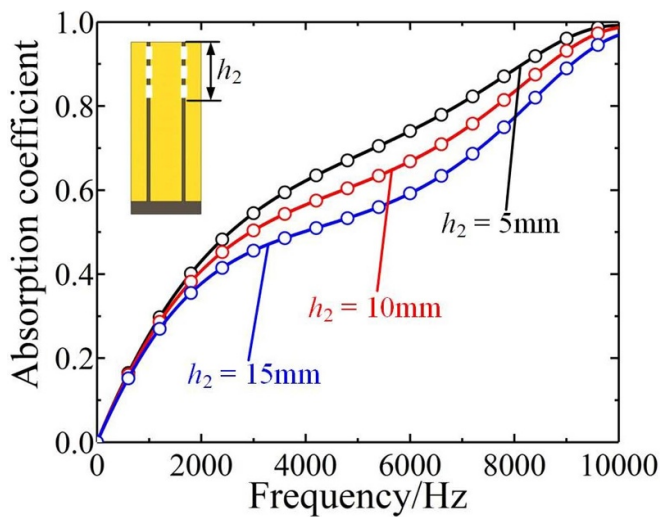


Figure 12. Influence of the length of defective segment on the sound absorption coefficient when the defect layer is at the top.

performance is similar to that of the thickness of the anechoic layer in figure 8(a).

5. Conclusion

A novel underwater composite anechoic layer inserted with periodically placed parallel steel plates has been proposed. A theoretical model for predicting its sound absorption is established and validated by comparing the predictions with FE simulation results. The influence of rubber properties and plate geometrical parameters on underwater sound absorption is systematically investigated. Main findings are summarized as follows:

- (a) For the first time, the complex viscosity model of viscoelastic materials is applied to characterize the acoustic performance of the proposed anechoic layer. In contrast with the complex modulus model, the shear wave is not considered as shear effects of the viscoelastic material are

reflected by the imaginary part of complex viscosity, thus simplifying the theoretical model.

- (b) Underwater absorption of the proposed anechoic layer is greatly improved relative to the structure purely made of rubber, for the inserted plates enlarge shear deformation of rubber at plate–rubber interfaces, causing more acoustic energy dissipation.
- (c) For enhanced absorption at low frequencies, the anechoic layer needs to have small acoustic impedance, which can be achieved by adjusting either the rubber density or the speeds of compressive and shear waves in rubber, or both.
- (d) Rubber viscosity and plate spacing play dominant roles in energy dissipation. Excessive viscosity would hinder rubber vibration, thus weakening the acoustic performance of the anechoic layer.
- (e) The presence of interfacial defect (e.g. non-tight connection) caused by the separation of rubber and plate insertions reduces the absorption performance of the anechoic layer. The closer the defect is located to the entrance, the more sensitive the absorption is to the defect.

Data availability statement

All data that support the findings of this study are included within the article (and any supplementary files).

Acknowledgments

This work was supported by the National Natural Science Foundation of China (52075416, 11772248, 11972185 and 12032010), and the Open Fund of the State Key Laboratory of Mechanics and Control of Mechanical Structures (MCMS-I-0219K01-02).

ORCID iDs

Mingyu Duan <https://orcid.org/0000-0002-8413-6751>
 Fengxian Xin <https://orcid.org/0000-0001-8855-5366>

References

- [1] Gaunard G 1977 One-dimensional model for acoustic absorption in a viscoelastic medium containing short cylindrical cavities *J. Acoust. Soc. Am.* **62** 298–307
- [2] Wen J, Zhao H, Lv L, Yuan B, Wang G and Wen X 2011 Effects of locally resonant modes on underwater sound absorption in viscoelastic materials *J. Acoust. Soc. Am.* **130** 1201–8
- [3] Li Y, Xu F, Lin Z, Sun X, Peng Q, Yuan Y, Wang S, Yang Z, He X and Li Y 2017 Electrically and thermally conductive underwater acoustically absorptive graphene/rubber nanocomposites for multifunctional applications *Nanoscale* **9** 14476–85
- [4] Pritz T 2009 Relation of bulk to shear loss factor of solid viscoelastic materials *J. Sound Vib.* **324** 514–9
- [5] Ivansson S M 2008 Numerical design of Alberich anechoic coatings with superellipsoidal cavities of mixed sizes *J. Acoust. Soc. Am.* **124** 1974–84
- [6] Yang H, Li Y, Zhao H, Wen J and Wen X 2014 Acoustic anechoic layers with singly periodic array of scatterers: computational methods, absorption mechanisms, and optimal design *Chin. Phys. B* **23** 283–91
- [7] Zhao D, Zhao H, Yang H and Wen J 2018 Optimization and mechanism of acoustic absorption of Alberich coatings on a steel plate in water *Appl. Acoust.* **140** 183–7
- [8] Yang H, Xiao Y, Zhao H, Zhong J and Wen J 2019 On wave propagation and attenuation properties of underwater acoustic screens consisting of periodically perforated rubber layers with metal plates *J. Sound Vib.* **444** 21–34
- [9] Theocaris P S 1969 Interrelation between dynamic moduli and compliances in polymers *Kolloid-Z. Z. Polymere* **235** 1182–8
- [10] Ivansson S M 2006 Sound absorption by viscoelastic coatings with periodically distributed cavities *J. Acoust. Soc. Am.* **119** 3558–67
- [11] Sharma G S, Skvortsov A, MacGillivray I and Kessissoglou N 2017 Acoustic performance of gratings of cylindrical voids in a soft elastic medium with a steel backing *J. Acoust. Soc. Am.* **141** 4694–704
- [12] Ye C, Liu X, Xin F and Lu T J 2018 Influence of hole shape on sound absorption of underwater anechoic layers *J. Sound Vib.* **426** 54–74
- [13] Zhong J, Zhao H, Yang H, Wang Y, Yin J and Wen J 2019 Theoretical requirements and inverse design for broadband perfect absorption of low-frequency waterborne sound by ultrathin metasurface *Sci. Rep.* **9** 1
- [14] Zhong J, Zhao H, Yang H, Yin J and Wen J 2019 On the accuracy and optimization application of an axisymmetric simplified model for underwater sound absorption of anechoic coatings *Appl. Acoust.* **145** 104–11
- [15] Hong-Gang Z, Yao-Zong L, Ji-Hong W, Dian-Long Y, Gang W and Xi-Sen W 2006 Sound absorption of locally resonant sonic materials *Chin. Phys. Lett.* **23** 2132–4
- [16] Zhao H, Liu Y, Wen J, Yu D and Wen X 2007 Tri-component phononic crystals for underwater anechoic coatings *Phys. Lett. A* **367** 224–32
- [17] Zhao H, Liu Y, Yu D, Wang G, Wen J and Wen X 2007 Absorptive properties of three-dimensional phononic crystal *J. Sound Vib.* **303** 185–94
- [18] Zhao H, Wen J, Yu D and Wen X 2010 Low-frequency acoustic absorption of localized resonances: experiment and theory *J. Appl. Phys.* **107** 1734
- [19] Meng H, Wen J, Zhao H, Lv L and Wen X 2012 Analysis of absorption performances of anechoic layers with steel plate backing *J. Acoust. Soc. Am.* **132** 69–75
- [20] Meng H, Wen J, Zhao H and Wen X 2012 Optimization of locally resonant acoustic metamaterials on underwater sound absorption characteristics *J. Sound Vib.* **331** 4406–16
- [21] Zhao H, Wen J, Yang H, Lv L and Wen X 2014 Backing effects on the underwater acoustic absorption of a viscoelastic slab with locally resonant scatterers *Appl. Acoust.* **76** 48–51
- [22] Wang Z, Huang Y, Zhang X, Li L, Chen M and Fang D 2020 Broadband underwater sound absorbing structure with gradient cavity shaped polyurethane composite array supported by carbon fiber honeycomb *J. Sound Vib.* **479** 115375
- [23] Kalso M A, Giacomini A J, Saengow C and Piette J H 2019 Macromolecular architecture and complex viscosity *Phys. Fluids* **31** 087107
- [24] Li S-P, Zhao G and Chen H-Y 2005 The relationship between steady shear viscosity and complex viscosity *J. Dispers. Sci. Technol.* **26** 415–9
- [25] Achenbach J D 1973 *Wave Propagation in Elastic Solids* (Amsterdam: North-Holland)
- [26] Maa D Y 2001 Theory of microslit absorbers *Chin. J. Acoust.* **25** 1–10
- [27] COMSOL Multiphysics® v. 5.4. COMSOL AB (Sweden: Stockholm) (available at: cn.comsol.com)